# NEW MnZn FERRITES AND THEIR APPLICATIONS

[1]Andrej Žnidaršič in [2]Miha Drofenik

[1]ISKRA FERITI, d.o.o., Ljubljana, Slovenia
[2]Univerza v Mariboru, Fakulteta za kemijo in kemijsko tehnologijo, Maribor, Slovenia

**Key words:** magnetic ceramic, MnZn ferrites, magnetic properties, electrical properties, microstructures, applications

**Abstract:** MnZn ferrites, ceramic with special magnetic properties, are widely used as core materials for inductive components in electronics. The demands of future electronic systems require solutions that improve efficiency, reduce weight and not add pollution to the environment. The requirements for component design are a smaller size, weight reduction, performance increase and durability. This paper describes the applications and properties of new designed matireals12Gi, 27G, 55G, 75G and 65G.

# Novi MnZn feriti in njihove aplikacije

**Kjučne besede:** magnetna keramika, MnZn feriti, magnetne lastnosti, električne lastnosti, mikrostruktura, aplikacije

**Izvleček:** MnZn feriti so keramični materiali z magnetnimi lastnostmi in sestavni deli induktivnih komponent namenjeni različnim aplikacijam v elektroniki. Trendi na področju elektronske industrije so usmerjeni v zmanjšanje teže osnovnih kompoment in izboljšanju osnovnih magnetnih lastnosti. Zahteve po zmanjšanju teže in prostornine novih induktivnih komponent narekujejo boljše lastnosti osnovnih materialov in večjo trajnost. V članku so predstavljene lastnosti novih materialov 12Gi, 27G, 55G, 75G in 65G ter njihova uporaba.

## 1. Introduction

Several improved materials will be discussed. It is important to select materials that are suited to specific applications. Some materials with their properties are listed:

1. EMI applications require a current compensated chokes which are very important to eliminate the disturbing interference sources. A ferrite material with a high initial permeability, high impedance over a broad frequency range and high operating temperature is required.
2. Splitter applications in ADSL applications required a plain old telephone system (POTS) splitter used to separate the high frequency data from low frequency voice signals. The core material must have a high reversible permeability at high magnetic field. In addition, a lower number of turns and smaller cores are required. This behavior can be achieved by high initial permeability and high saturation of the ferrite materials.
3. As electronic modules become smaller and lighter, the power supplies must likewise be reduced. The core losses, consisting of hysteresis losses, eddy current losses and residual losses, vary considerably with operating frequency and magnetic flux density. The losses can be reduced by a uniform microstructure and high material resistivity. But low mechanical stress, low magneto crystalline anisotropy and low magnetostriction are also required.
4. DSL applications require a fast data transfer without distortion. Inductive components are used in the customer^x^s premises modem and central office line transformers to realize a distortion free digital signal transmission along the copper wire of the conventional telephone network. The main target for the inductive cores is a long reach (higher than 5 km) at a high data distance.

## 2. Ferrite technology

The first step is the production of granulated ferrite powder. The weighed raw materials iron oxide, manganese oxide and zinc oxide are mixed and then palletized with a small amount of water. The red pellets with a pellet size of 3-5 mm are calcinated in a rotary kiln at about 1000$^0$C. Here the oxides react partly to the magnetic ferrite with spinel structure. After that the black pellets, water and some inorganic additives (amount from 0.01 - 0.1wt%) are added into an attritor for fine milling. The inorganic additives are necessary to improve the sintering behavior and/or the magnetic properties. The second part of the technology important to improve properties in associated with core shapes, sintering of them in the temperature range 1200 - 1400$^0$C and grinding of final cores.

## 3. Design principles

The performance of ferrites is not determined only by a high initial permeability. Other characteristics such as low losses, high saturation flux density, high sintered density and frequency characteristics are also important. In many cases, these requirements are not satisfied at the same time, so a compromise material has to be selected in such cases.

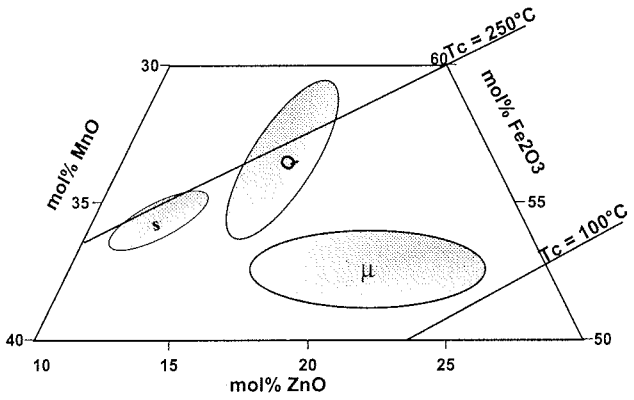


*Fig. 1: Composition diagram for MnZn ferrites*

The high initial permeability of materials depends to a large extent on the mobility of the Bloch's domain walls. To obtain high permeability it is important to lower the anisotropy and the magnetostriction. During the development of high-permeability MnZn ferrites much effort was devoted to the parameters which govern the bulk properties such as composition, microstructure and porosity /1/. To achieve a high permeability the composition of MnZn ferrite must be selected from a relatively narrow composition range, figure 1, region μ, where a zero crystalline anisotropy and a zero average magnetostriction can be expected. Studies of the grain-boundary chemistry in combination with grain-boundary structural analysis revealed that the grain boundaries are characterized by ZnO evaporation and the presence of a glassy phase and the segregation of various cations /2/. Firing conditions and additives are also important for achieving good properties. Well-adjusted sintering conditions support the development of the proper microstructure and the resulting magnetic properties. All these points have to be optimized in order to obtain desired magnetic properties.

Ferrites for power applications must be compositionally batched, figure 1 $B_{sat}$ region, and processed for low losses. Low power loss MnZn ferrites should have uniformly sized grains and high saturation density. The use of additives, a well-controlled process and a suitable sintering profile must be selected to decrease the power loss of ferrites. Additives and impurities are responsible for the grain-boundary chemistry and have a remarkable effect on the grain boundaries properties, particularly on the grain-boundary resistance /3/. In order to obtain a sintered body of uniformly sized fine grains, which would be suitable for achieving low power losses, grain growth should be suppressed especially in the initial stage of sintering process /4,6/. The selection of high-grade raw materials, with a defined low level of impurities, is of special importance in the production of MnZn ferrites for optimized microstructure properties. Addition of Ca and Si are well known to control the micro structural properties. Both ions strongly influence the microstructure of MnZn ferrites. Furthermore, the total resistance of MnZn ferrites increases due to the precipitation of silicate phases at the grain boundaries. This has the advantage that CaO and $SiO_2$ are doped in a defined amount in the ferrite mixture and their effect can be optimized in order to control the grain size and resistivity. In addition to the concentration of impurities, the reactivity of raw materials is a fundamental importance to control and optimize the production process /5/.

The total usable flux, AC + DC, in single ended power supplies is becoming important. The usable flux of a ferrite material is closely connected with the saturation flux density $B_s$, which in turn depends on the composition and density of the ferrite. For practical purposes, the composition of a ferrite material has to be considered as a compromise between application temperature (the position of the secondary permeability maximum corresponding to the position of minimum core losses) and required saturation flux density (which falls as temperature rises). Detailed investigation of core loss mechanisms has made it possible to develop new ferrite materials for various applications.

## High saturation power ferrite 55G

55G is intended for output chokes in power supplies. The requirement of a high saturation level to accommodate a high dc current is necessary to avoid saturating the core. The energy storage value of a choke is proportional to the square of peak flux density and determines the core volume required. Whenever space is limited, this is an important consideration. The new Iskra Feriti material 55G is usable to 500 kHz and above /8/.

***Table 1:** 55G Material characteristics*

| *Parameter* | *measuring conditions* | *value* |
|---|---|---|
| $\mu_i$ [] | 25 °C, 10 kHz, 0.1 mT | 1800 ± 20% |
| $B_S$ [mT] | 25 °C, 10 kHz, 1200 A/m | ≥ 510 |
| | 100 °C, 10 kHz, 1200 A/m | ≥ 430 |
| | 120 °C, 10 kHz, 1200 A/m | ≥ 400 |
| $T_c$ [°C] | | ≥ 240 |

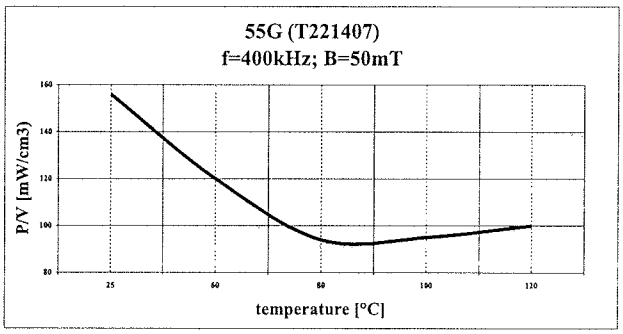


*Fig. 2: Power losses versus temperature*

Preferred applications are:

- High current output chokes - wherever space is at premium like a low profile converter modules, core volume can be reduced. The advantage increases with temperature.

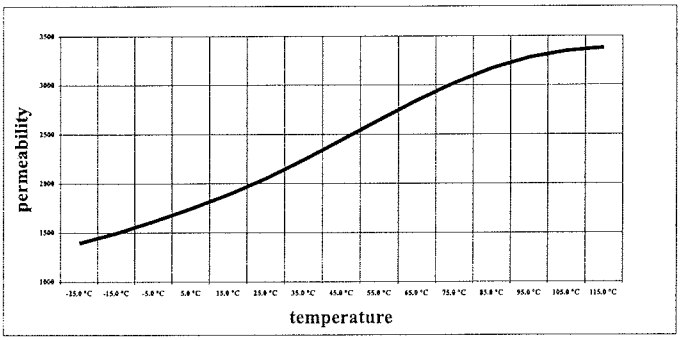


*Fig.3: Initial permeability versus temperature*

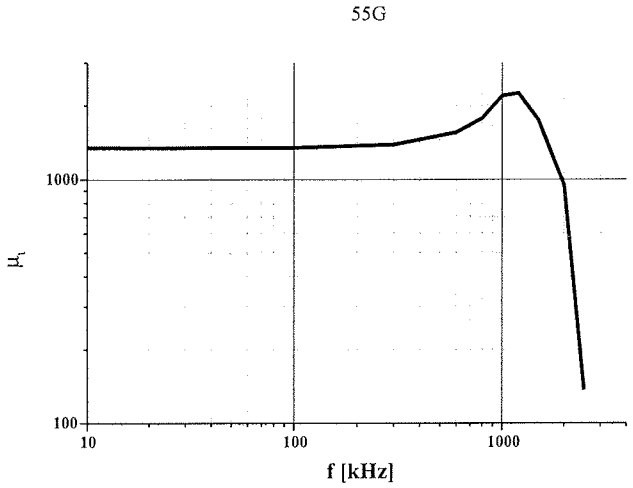


*Fig. 4: Initial permeability versus frequency*

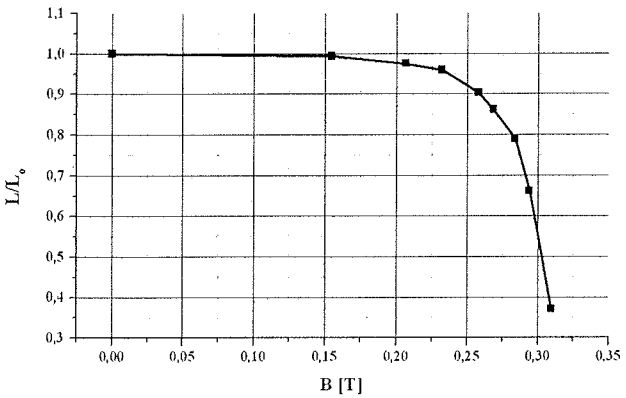


*Fig. 5: Inductance as function of $B_{pmax}$ at 120°C*

- High voltage ignition transformers - for example in electronic lighting ballast where high flux density occurs during ignition, but losses have to be low during steady state operation.
- Gapped toroids where high-energy storage is required.

## High frequency power ferrite 75G

The increase in electrical applications for the automotive market is stressing the 12 volt system. The way to solve the insufficient electrical power is to increase the 12V standard to a 42V standard. The additional requirement to reduce weight and change to a drive by wire concept opens the market for voltage converters. The operating frequency of these converters will be about 500 Hz to 1MHz. The right material is a high frequency power grade, like our 75G, Table2 and Figures 6 to 9. The ferrite components that will be needed for various applications could use 2 planar core sets, one for transformer and one for the output choke for the core solution.

***Table 2:** 75G Material characteristics*

| *Parameter* | *measuring conditions* | *value* |
|---|---|---|
| $\mu_i$ [] | 25 °C, 10 kHz, 0.1 mT | 1300 ± 20% |
| $B_S$ [mT] | 25 °C, 10 kHz, 1200 A/m | ≥ 510 |
| | 100 °C, 10 kHz, 1200 A/m | ≥ 430 |
| | 120 °C, 10 kHz, 1200 A/m | ≥ 400 |
| $T_c$ [°C] | | ≥ 240 |

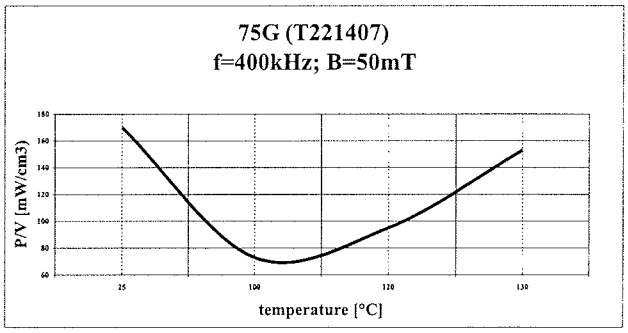


*Fig. 6: Power loss versus temperature*

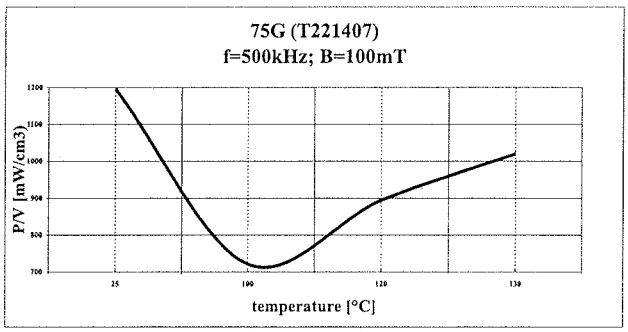


*Fig. 7: Power loss versus temperature*

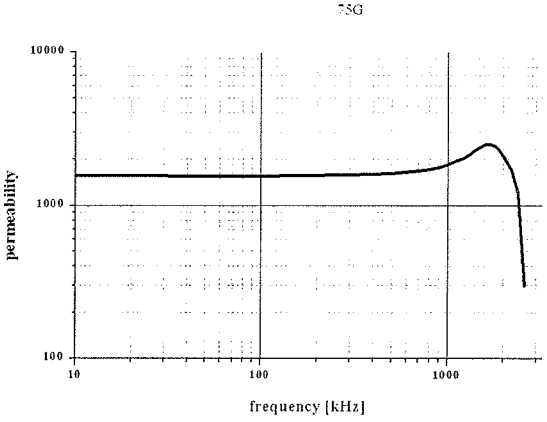


*Fig. 8: Initial permeability versus frequency*

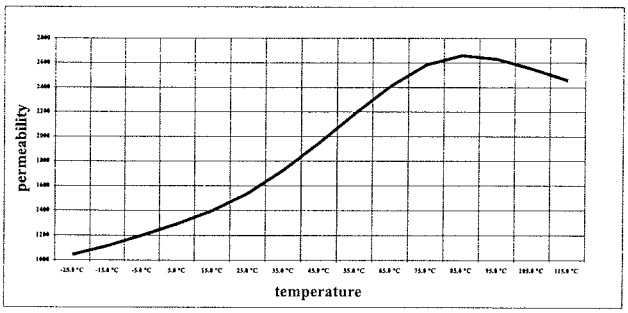


*Fig. 9: Initial permeability versus temperature*

Some potential applications under the 42V system are:

- Lighter, smaller and more efficient air conditioning
- Higher efficiency, longer life, water pump
- Faster starter, superior charging starter/alternator
- Mobile office: fax, PC,....

## Power material 65G – new level of power density

The properties of 65G, a new high flux density power material suitable for frequency up to 400 kHz is shown in Table 3 and Figures 10 to 13. This material is primarily intended for output chokes in power supplies where a high saturation level is required to accommodate DC + AC currents at elevated temperatures. The energy storage volume of a choke is proportional to the square of peak flux density and determines the core volume required. When space is limited, this is an important consideration.

***Table 3:*** *65G Material characteristics*

| *Parameter* | *measuring conditions* | *value* |
|---|---|---|
| $\mu_i$ [] | 25 °C, 10 kHz, 0.1 mT | 2300 ± 20% |
| $B_S$ [mT] | 25 °C, 10 kHz, 1200 A/m | ≥ 510 |
| | 100 °C, 10 kHz, 1200 A/m | ≥ 380 |
| | 120 °C, 10 kHz, 1200 A/m | ≥ 360 |
| $T_c$ [°C] | | ≥ 210 °C |

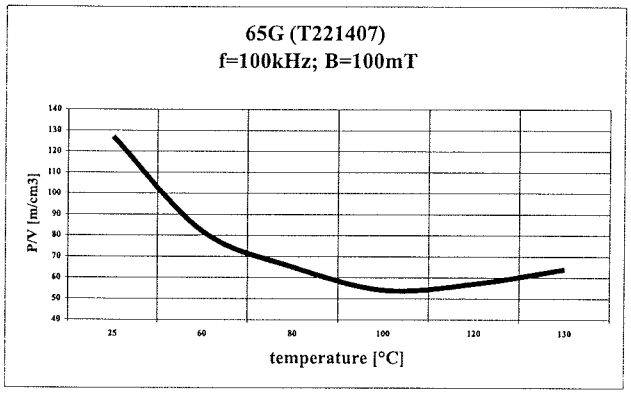


*Fig. 10: Power losses versus temperature*

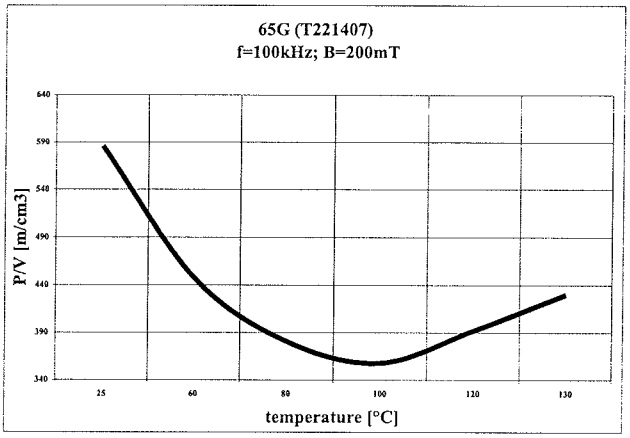


*Fig. 11: Power losses versus temperature*

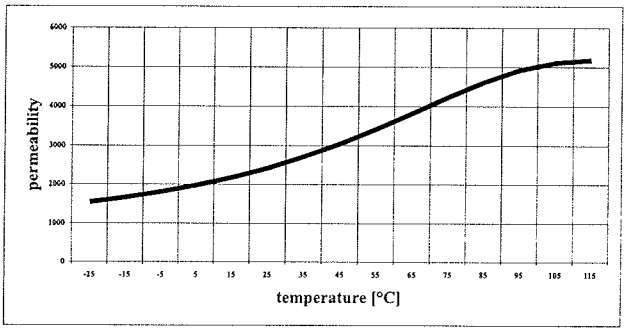


*Fig. 12: Permeability versus temperature*

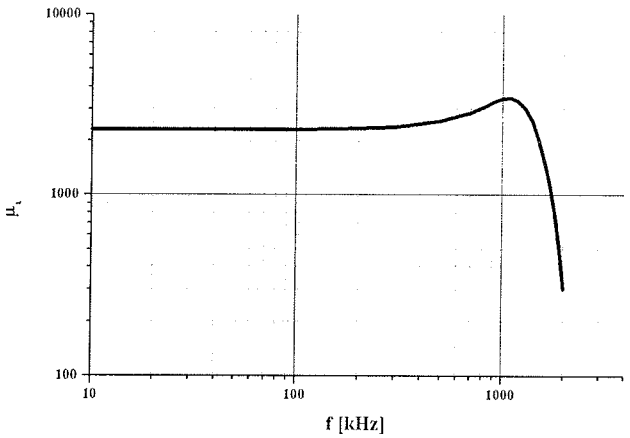


*Fig. 13: Permeability versus frequency*

Some potential applications are automotive electronics and electronic lighting ballasts.

## Innovative material 12Gi for (A) XDSL interface transformers

The ferrite producer Iskra- Feriti has developed an improved 12i ferrite material optimized for (A) XDSL applications. In comparison with conventional 12G ferrite material, the new 12Gi, Table 4 and Figures 14 and 15, allows for increases in the data rate transfer and distance covered by (A)XDSL lines.

The THD, Total Harmonic Distortion, of a ferrite component should be low under operating conditions. THD is a function of flux density (B), frequency (f) and temperature (T). To evaluate the material quality with respect to THD an audio analyzer was used on toroid samples. The improved 12Gi is optimized by low impurity raw materials, the addition of additives and improved processing and sintering conditions.

***Table 4:*** *12Gi Material characteristics*

| *Parameter* | *measuring conditions* | *value* |
|---|---|---|
| $\mu_i$ [] | 10 kHz, 25 °C, 0.1 mT | 10000 ± 20% |
| $\eta_B$ [$10^{-3}$/T] | 10 kHz, 25 °C, 1.5-3.0 mT | < 0.15 |
| tgδ/μi [10-6] | 10 kHz, 25 °C, 0.1 mT | ≤ 7 |
| | 100 kHz, 25 °C, 0.1 mT | ≤ 40 |
| αF [106/K] | 25 - 55 °C | -1 -+ 1 |
| TC [°C] | | ≥ 130 |

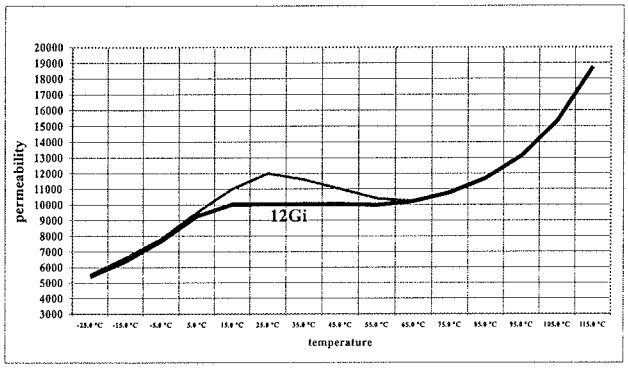


*Fig. 14: Permeability versus temperature*

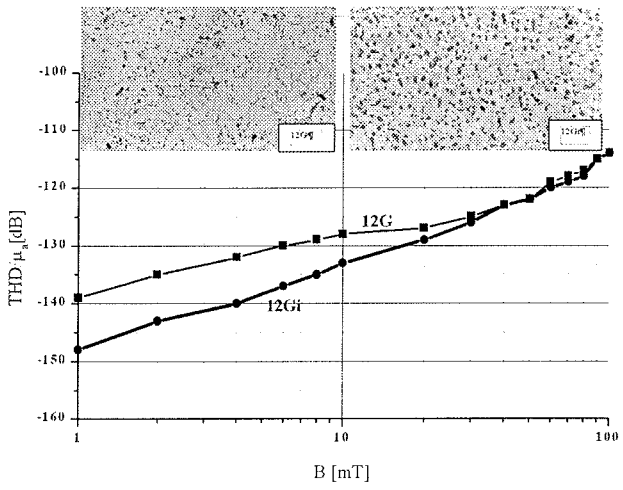


*Fig.15: THD/$\mu_a$ versus B for 12G and new 12Gi at 20 kHz*

## New material 27G for splitter applications

27G material, Table 5 and Figures 16 to 18, replaces 25G material in splitter (POTS) applications. 27G material is the first MnZn-ferrite which is available in production and combines both a high permeability and high saturation,. Both the high permeability and the high saturation at room temperature lead to the improvement of the DC-bias behavior.

This innovative material will also be of interest for interference suppression in automotive electronics and in frequency converters for industrial applications.

Typical industrial applications are found in pumps, fans, conveyer belt drivers, textile machinery and printing presses.

Suppression of this interferences is now a statutory requirement and calls for filters that can cope with high power outputs. The high power outputs inevitably cause high operating and ambient temperatures. The filters therefore require ferrite materials with high initial permeability and high magnetic saturation. The new 27G material is particularly suitable for these extreme requirements.

***Table 5:*** *27G Material characteristics*

| *Parameter* | *measuring conditions* | *value* |
|---|---|---|
| $\mu_i$ [] | 25 °C, 10 kHz, 0.1 mT | 3800 ± 20% |
| $B_S$ [mT] | 25 °C, 10 kHz, 1200 A/m | ≥ 530 |
| | 100 °C, 10 kHz, 1200 A/m | ≥ 410 |
| | 120 °C, 10 kHz, 1200 A/m | ≥ 370 |
| $T_c$ [°C] | | ≥ 210 |

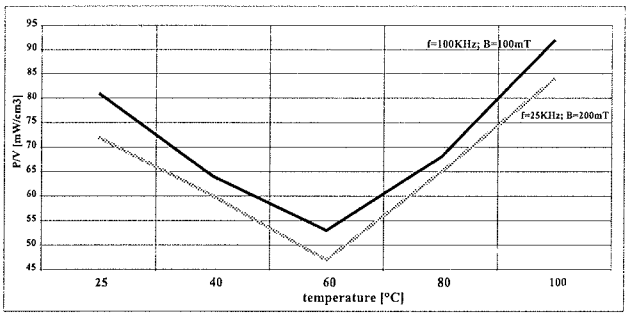


*Fig. 16: Power loss versus temperature*

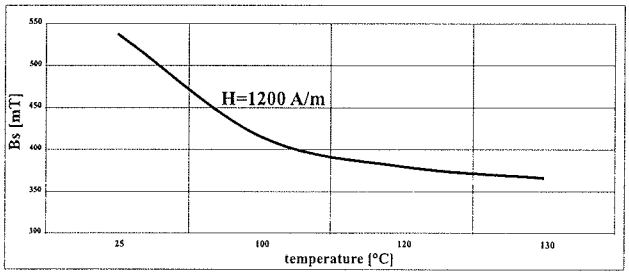


*Fig. 17: Saturation flux density versus temperature*

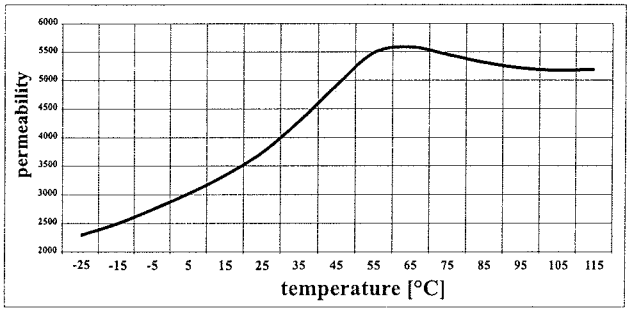


*Fig. 18: Permeability versus temperature*

All materials were successfully introduced on production and available in different core shapes.

## 3. Conclusion

The technical demand for improved soft ferrites has been growing. The technical department at Iskra - Feriti, has been busy developing and improving new ferrites to meet these demands. These materials meet the demands in both quantity and applications requirements that demand improved performance. Raw materials, the improvements in manufacturing technology and the ability to measure the results, play a decisive role in improving the quality and lowering the costs of ferrites. The results of these developments are expected to give new impulses for electrotechnical applications.

## 4. References

/1/ Goldman, »Modern Ferrite Technology«, Van Nostrand Reihold 1990, New York

/2/ M.Drofenik, A.Žnidaršič, D.Makovec, »Influence of Addition of $Bi_2O_3$ on the Grain Boundary of MnZn Ferrites«, J.Am.Cer.Soc., 82 (11) 2841 - 48 (1998)

/3/ M.Drofenik, A.Žnidaršič, I.Zajc, »Highly resistive grain boundaries in doped MnZn ferrites for high frequency power supplies«, J. Appl. Phys., vol 82, No.1 333 - 340 (1997)

/4/ A.Žnidaršič, M.Drofenik, »Influence of oxygen partial pressure during sintering on the power loss of MnZn ferrites«, IEEE Trans. Mag. 32(3), 1941 - 45 (1996)

/5/ A.Žnidaršič, M.Drofenik, »Modern developments trends in high-performance soft ferrites«, Inf. MIDEM, 32(2), 95 - 99 (2002)

/6/ M.Drofenik, A.Žnidaršič, D.Makovec, »Stabilization of MnZn ferrites by re-oxidation of their grain boundaries«, Z. Met. kd, vol 92, 110 - 114 (2001)

/7/ M.Drofenik, A.Žnidaršič, D.Makovec, "Ca redistribution in MnZn ferrites grain boundaries during heat treatment in reducing atmosphere", ICF8, main conference, 286-287, Kyoto, Japan (2000)

/8/ A.Žnidaršič, M.Drofenik, "A new power MnZn ferrite for DC -DC applications", Apec., Seventeenth Annual IEEE, Applied Power Electronics, Conference and Exposition, vol. 1, Dallas, Texas (2002)

*Doc. Dr. Andrej Žnidaršič*
*Iskra Feriti, d.o.o.*
*Stegne 29, 1521 Ljubljana*

*Prof. Dr. Miha Drofenik*
*Univerza v Mariboru,*
*Fakulteta za kemijo in kemijsko tehnologijo,*
*Smetanova 17, 2000 Maribor*

*Prispelo (Arrived): 11.12.2003* *Sprejeto (Accepted): 25.02.2004*

# THE INTERACIONS OF CONDUCTIVE AND GLASS PHASE IN THICK-FILM RESISTORS DURING FIRING

[1]Marko Hrovat, [2]Darko Belavič, [1]Janez Holc, [1]Janez Bernard, [1]Andreja Benčan, [1]Jena Cilenšek

[1]Jozef Stefan Institute, Ljubljana, Slovenia
[2]HIPOT-R&D d.o.o., Sentjernej, Slovenia

**Key words:** thick-film resistors, characterisation, ruthenium oxide, ruthenates, phase equilibria

**Abstract:** Some thick-film resistors based on $RuO_2$, ruthenates or a mixture of $RuO_2$ and ruthenates, were evaluated. The resistors were fired at different temperatures to determine the influence of firing temperature on the electrical and microstructural characteristics. The microstructures of the thick-film resistors were analysed with scanning electron microscopy and energy-dispersive X-ray analysis. The temperature coefficients of resistivity, noise indices and gauge factors were measured as a function of firing temperature. After a long term high temperature firing ruthenate based conductive phase transform into $RuO_2$ coinciding with a significant increase of the temperature coefficients of resistivity and decrease of the resistance. Glass phase in thick-film resistors was analysed by EDS. All glass compositions are rich in $SiO_2$ with the molar ratio $SiO_2$ / PbO between 2 and 2.5. Subsolidus equilibria in the $RuO_2$ - PbO - $SiO_2$ diagram were determined with the aim to verify the interactions between conductive phase (either ruthenium oxide or ruthenate) and silica-rich glasses. The tie line between $RuO_2$ and $PbSiO_3$ indicates that the lead ruthenats are not stable in the presence of the silica-rich glass phase.

# Interakcije med prevodno in stekleno fazo v debeloplastnih uporih med procesom žganja

**Kjučne besede:** debeloplastni upori, karakterizacija, rutenijev oksid, rutenati, fazni diagrami

**Izvleček:** Karakterizirali smo nekatere debeloplastne uporovne materiale na osnovi $RuO_2$, rutenatov ali zmesi $RuO_2$ in rutenatov. Uporte smo žgali pri različnih temperaturah, da bi ugotovili vpliv temperature žganja na električne in mikrostrukturne karakteristike. Mikrostrukture debeloplastnih uporov so bile preiskane z elektronskim vrstičnim mikroskopom in rentgensko analizo. Izmerili smo temperaturne koeficiente upornosti, indekse tokovnega šuma in faktorje gauge v odvisnosti od temperature žganja. Ugotovili smo, da v debeloplastnih uporih, žganih dolgo časa pri povišanih temperaturah, rutenat preide v rutenijev oksid. Pri tem se zelo zniža plastna upornost in poviša temperaturni koeficient upornosti. Stekleno fazo v debeloplastnih uporih smo analizirali z EDS (Energy Disspersive X-ray Analysis). Ugotovili smo, da so vsa stekla bogata na $SiO_2$ z razmerjem $SiO_2$ / PbO med 2 in 2,5. Preiskali smo fazna ravnotežja v sistemu $RuO_2$ - $SiO_2$ - PbO. Rezultati so potrdili, da rutenat ni stabilen v prisotnosti stekel bogatih na $SiO_2$.

## Introduction

Thick-film resistors consist basically of a conducting phase, a lead-borosilicate-based glass phase and an organic vehicle. The organic material is burned out during the high-temperature processing. The ratio between the conductive and the glass phases roughly determines the specific resistivity of the resistor. In most modern resistor compositions the conductive phase is either $RuO_2$ or ruthenates; mainly, as reported in the literature, lead or bismuth ruthenates. The main change during firing is the transition from a mixture of glass grains and, usually, much finer grains of the conductive phase in a thick-film paste, into conductive chains through the sintered glass in the fired resistor. During the firing cycle all the constituents of the resistor paste react with each other and the melted glass also interacts with the substrate The resistors are only a relatively short time (typically 10 min) at the highest temperature (typically 850°C). Because of this the reactions between the constituents of the resistor material do not reach equilibrium so that the required characteristics of fired materials (e.g long-term stability, low noise indices and a low temperature coefficient of resistivity) are, in a way, a compromise as a consequence of this frozen non-equilibrium /1-5/. The aim of this paper is to present the results on some thick film resistor material, fired either at the required 850°C for 10 min or at higher firing temperatures for significantly longer times. The aim was to gain some insight into the changes in the electrical and microstructural characteristics, and gauge factors if the resistors are fired long enough at the high temperature to allow the reactions within the resistor to reach the equilibrium. Thick-film resistors with a nominal resistivity of 10 kohm/sq. (Du Pont 8039 and 2041, and Heraeus 8241) were evaluated. The conductive phase in 8039, 2041 and 8241 resistors is based on $(Bi_{2-x}Pb_x)Ru_2O_{7-x/4}$, a mixture of $RuO_2$ and $Pb_2Ru_2O_{6.5}$, and $RuO_2$, respectively /6,7/. Data on the conductive phase and the qualitative results of an energy-dispersive X-ray analysis (EDS) of the glass composition of the thick-film resistors are summarized in Table 1. All glasses contain, as main elements, lead, silicon and aluminum oxides. Boron oxide, which is also present in the glass phase, cannot be detected in the EDS spectra because of the low relative boron weight fraction in the glass and the strong

absorption of the boron $K_\alpha$ line during EDS analysis in the glass matrix.

**Table 1.** Conductive phase and qualitative results of EDS microanalysis of elements detected in glass phase of thick-film resistors /17/.

| Resistor | Conductive phase | Ma in elements | Other elements detected |
|---|---|---|---|
| 8039 | ruthenate | Si, Pb, Al | Zr |
| 2041 | RuO 2+ ruthenate | Si, Pb, Al | Mg, Zn, Ca, Ba |
| 8241 | RuO 2 | Si, Pb, Al | Zn, Cu |

The X-ray analysis of conductive phase in investigated thick film resistors will be given. The change of conductive phase (from ruthenate to the ruthenium oxide) at high firing temperatures, depending on the composition of glass phase will be discussed.

## Experimental

Thick-film resistors with dimensions 1.6x1.6 $mm^2$ were printed on 96% alumina substrates and fired for10 min at 850°C and for 6 hours at 950°C. The resistors were terminated with a Pd/Ag conductor that was prefired at 850°C. Cold TCRs (from -25°C to 25°C) and hot TCRs (from 25°C to 125°C) were calculated from resistivity measurements at - 25°C, 25°C, and 125°C. Current noise was measured in dB on 100 mW loaded resistors by the Quan Tech method (Quan Tech Model 315-C). Gauge factors (GFs) were measured. The resistors were examined by X-ray powder-diffraction (XRD) analysis A JEOL JSM 5800 scanning electron microscope (SEM) equipped with an energy-dispersive X-ray analyser (EDS) was used for the microstructural analysis.

## Results and discussion

Sheet resistivities, cold (-25°C to 25°C) and hot (25°C to 125°C) TCRs, noise indices and gauge factors of the investigated thick-film resistors that were 10 min at 850°C and 6 hours at 950°C are shown in Table 2.

After firing at 950°C for 6 hours, the resistivities of all the resistors significantly decreased to around 5% of the resistivities after firing at 850°C for the 2041 resistors, and to 1% or less for the 8039 and 8241 resistors. The GFs of all the resistors, as well as the sheet resistivities, decreased with increasing firing temperature. The TCR values of the resistors after firing at the "normal" temperature of 850°C are below $100x10^{-6}/K$. After firing for 6 hours at 950°C the absolute values of the TCRs of the 8039 and 8241 resistors increased significantly. The noise indices decrease with increased firing temperature. The 2041 resistor material has the lowest noise, around or under -20 dB, regardless of the firing temperature.

X-ray diffraction (XRD) spectra of ruthenate-based "equilibrated" resistors showed that at higher firing temperatures the ruthenate decomposes forming $RuO_2$, while the conductive phase in $RuO_2$-based resistors stays unchanged. This is shown in Figs. 1.a, 1.b and 1.c for 10 kohm/sq. Du Pont 8039 and 2041 thick film resistors, and Heraeus 8241 thick-film resistors, respectively /6/. As mentioned before, the 8241 resistor is based on $RuO_2$ and the 2041 material is based on a mixture of (mainly) ruthenate and $RuO_2$. The resistors were fired for 10 min at 850°C and for 6 hours at 950°C. After 6 hours of firing at 950°C the ruthenate peaks of the 8039 resistors disappear while the spectrum of $RuO_2$ based 8241 resistors remains unchanged. Presumably because of the interaction with the molten glass the ruthenate decomposes.

The decomposition of the ruthenate phase in the ruthenate-based 8039 resistor after high-temperature firing and the formation of $RuO_2$ was confirmed with SEM. Microstructures of the 8039 resistors that were fired for 10 min at 850°C and for 6 hours at 950°C are as an example in Figs. 2.a and 2.b. The microstructure of the 8039 resistor, fired at 850°C (Fig. 3.a) consists of light sub micrometer-sized particles of a conductive phase in a grey glass matrix. The dark particles are $SiZrO_4$. After 6 hours firing

**Table 1:** Sheet resistivities, cold and hot TCRs, noise indices and gauge factors of the thick-film resistors, fired 10 min at 850°C and 6 hours at 950°C

| Resistor | T firing (°C) | Resistivity (ohm/sq.) | Cold TCR (10-6/K) | Hot TCR (10-6/K) | Noise (dB) | GF |
|---|---|---|---|---|---|---|
| 8039 | 850 | 7,3 k | 50 | 90 | -14.3 | 11.0 |
| | 950, 6 h | 37 | 1845 | 1810 | -29.9 | 1.5 |
| 2041 | 850 | 6.6 k | -35 | 20 | -23.3 | 11.0 |
| | 950, 6 h | 280 | -90 | -85 | -32.0 | 7.0 |
| 8241 | 850 | 5.4 k | 20 | 60 | -4.5 | 15.5 |
| | 950, 6 h | 36 | 1950 | 1990 | -25.5 | 2.0 |

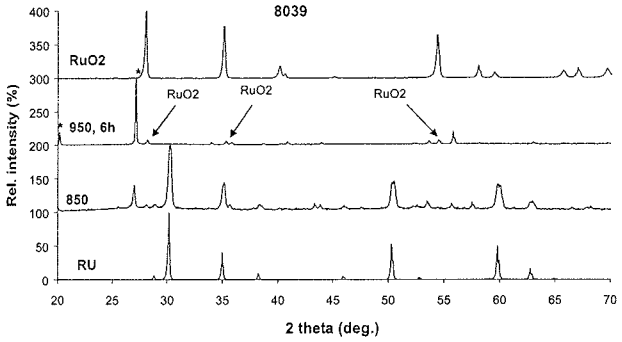


*Fig. 1a: XRD spectra of 2039 thick-film resistor, fired for 10 min at 850°C and for 6 hours at 950°C. Spectra of ruthenate (RU) and of $RuO_2$ (RuO2) are also included.*

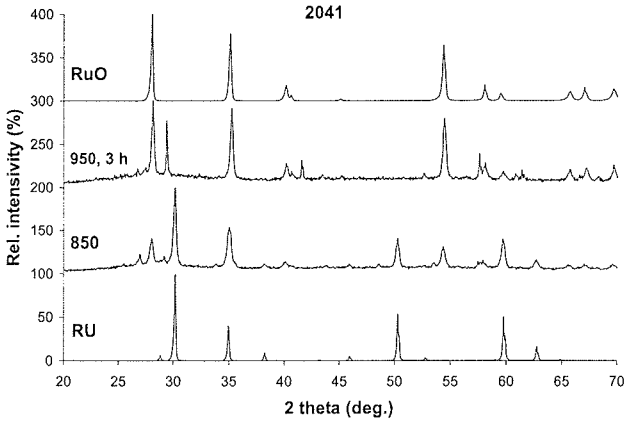


*Fig. 1b: XRD spectra of 2041 thick-film resistor, fired for 10 min at 850°C and for 6 hours at 950°C. Spectra of ruthenate (RU) and of $RuO_2$ ($RuO_2$) are also included.*

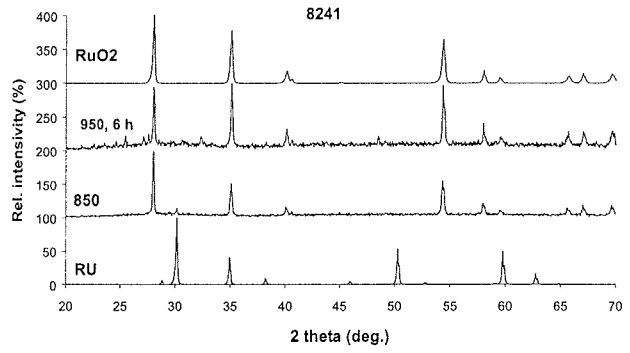


*Fig. 1c: XRD spectra of 8541 thick-film resistor, fired for 10 min at 850°C and for 6 hours at 950°C. Spectra of ruthenate (RU) and of $RuO_2$ (RuO2) are also included.*

at 950°C the ruthenate particles in the 8039 resistor have nearly all disappeared.

Adachi and Kuno /8,9/ studied high-temperature interactions between $PbO-B_2O_3-SiO_2$ glasses and $Pb_2Ru_2O_{6.5}$

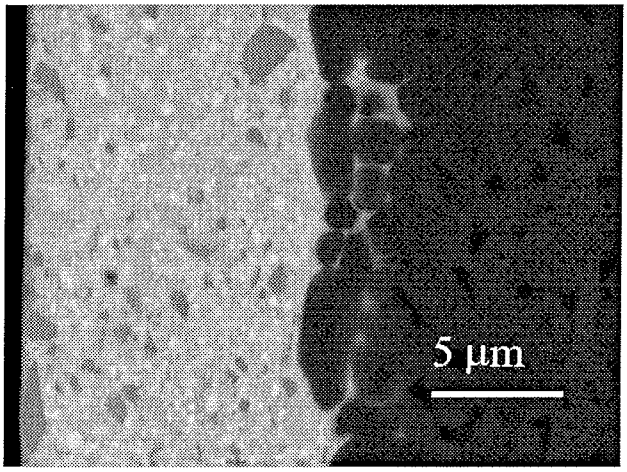


*Fig.2a: Microstructure of a cross-section of the thick-film resistor 8039, fired for 10 min at 850°C. Alumina substrate is on the right. Light particles are conductive phase - $(Bi_{2-x}Pb_x)Ru_2O_{7-x/4}$.*

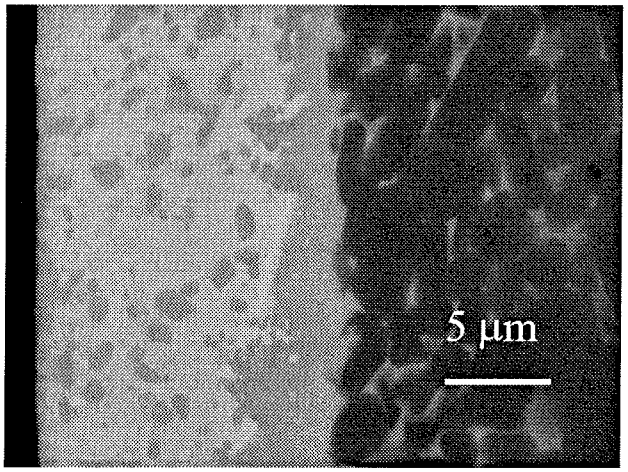


*Fig. 2b: Microstructure of a cross-section of the thick-film resistor 8039, fired for 6 hours at 950°C. Alumina substrate is on the right. After firing at 950°C the ruthenate particles in the 8039 resistor have nearly all disappeared.*

or $RuO_2$. They showed that in glasses poor in PbO the $Pb_2Ru_2O_{6.5}$ disappears and the $RuO_2$ is formed while for PbO-rich glasses the $RuO_2$ reacts with the PbO from the glass and forms $Pb_2Ru_2O_{6.5}$. Their results are summarised in Fig. 3. Three regions are marked in the $PbO-B_2O_3-SiO_2$ phase diagram. In the first region in the silica rich part of diagram ruthenates decomposes into $RuO_2$. In third region (PbO rich) ruthenates are stable while $RuO_2$ reacts with glass forming $Pb_2Ru_2O_{6.5}$. In glasses with roughly 1/1 $SiO_2$ / PbO ratio (second region) the $RuO_2$ and the ruthenate coexist.

To confirm these findings, the subsolidus ternary phase diagram of the $RuO_2$ - PbO - $SiO_2$.system was investigated. The glass phase in different commercial thick-film resistors was analysed by SEM and the $PbO/SiO_2$ ratio was

determined. All analysed glass compositions are rich in $SiO_2$ with the molar ratio $SiO_2$ / PbO between 2 and 2.5. The molar ratio $SiO_2$ / PbO in glass phases of thick-film resistors is also graphically shown as a short bold bar near $SiO_2$ in the PbO-poor part of the $RuO_2$ - PbO - $SiO_2$ system in Fig. 4. The PbO-rich part of phase diagram, which was not investigated, is shown with dotted lines. No ternary compound was found in the system. There is no binary compound between $RuO_2$ and $SiO_2$. The tie lines are between $Pb_2Ru_2O_{6.5}$ and $PbSiO_3$, and between $RuO_2$ and $PbSiO_3$. The results therefore indicate that the lead-ruthenate-based conductive phase in thick-film resistors is indeed unstable when in contact with the silica-rich glass phase, as shown by dashed lines in Fig. 4.

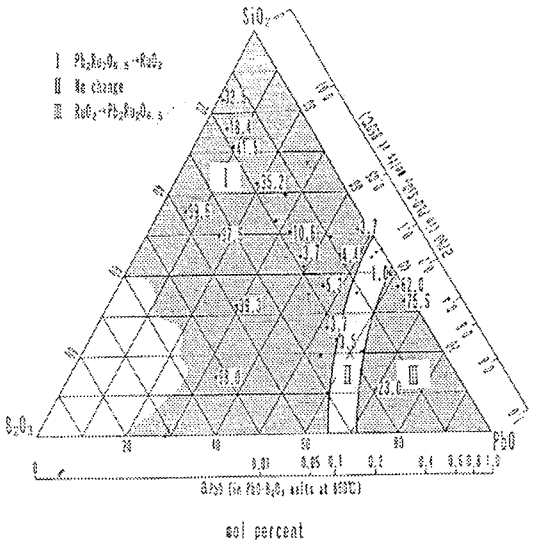

*Fig. 3: The PbO-$B_2O_3$-$SiO_2$ system (after Adachi and Kuno /8/). Lead ruthenate is stable in the region III and unstable in the region I.*

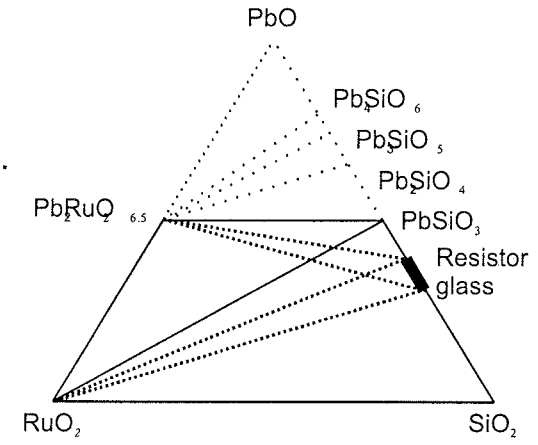


*Fig. 4: The proposed subsolidus ternary phase diagram of the PbO-poor part of the $RuO_2$ - PbO - $SiO_2$. The molar ratio $SiO_2$ / PbO in glass phases of some thick-film resistors is shown as a short bold bar near $SiO_2$ in the PbO-$SiO_2$ system.*

## Acknowledgement

The financial support of the Ministry of Education, Science and Sport of the Republic of Slovenia is gratefully acknowledged.

## References

/1./ J. W. Pierce, D. W. Kuty, J. L. Larry, The chemistry and stability of ruthenium based resistors, Solid State Technol., 25, (10), (1982), 85-93

/2./ R. W. Vest, "Materials science of thick-film technology", Ceram. Bull., 65, (4), (1986), 631-636

/3./ T. Inokuma, Y. Taketa, "Control of electrical properties of RuO2 thick film resistors", Active and Passive Elect. Comp., 12, (3), (1987), 155-166

/4./ O. Abe, Y. Taketa, M. Haradome, The effect of various factors on the resistivity and TCR of RuO2 thick film resistors - relation between the electrical properties and particle size of constituents, the physical properties of glass and firing temperature, Active and Passive Elect. Comp., 13, (2), (1988), 76-83

/5./ M. Hrovat, Z. Samardžija, J. Holc, D. Belavič, Microstructural, XRD and electrical characterization of some thick film resistors, J. Mater. Sci.: Materials in Electronics, 11, (3), (2000), 199-208

/6./ M. Hrovat, D. Belavič, Z. Samardžija, J. Holc, A characterisation of thick film resistors for strain gauge applications, J. Mater. Sci., 36, (11), (2001), 2679-2689

/7./ M. Hrovat, A. Benčan, D. Belavič, J. Holc, G. Dražič, The influence of firing temperature on the electrical and microstructural characteristics of thick film resistors for strain gauge applications, Sensors Actuators A, 103, (2003), 341-352

/8./ K. Adachi, H. Kuno, Decomposition of ruthenium oxides in lead borosilicate glass, J. Am. Ceram. Soc., 80, (5), (1997), 1055-1064

/9./ K. Adachi, H. Kuno, Effect of glass composition on the electrical properties of thick film resistors, J. Am. Ceram. Soc., 83, (10), (2000), 2441-2448

*Marko Hrovat, Janez Holc, Janez Bernard,*
*Andreja Benčan, Jena Cilenšek*
*Jozef Stefan Institute,*
*Ljubljana, Slovenia*

*Darko Belavič*
*HIPOT-R&D d.o.o., Sentjernej,*
*Slovenia*

*Prispelo (Arrived): 21.07.2003* *Sprejeto (Accepted):25.02.2004*

# PROBLEM NEPONOVLJIVOSTI SIMULACIJ ELEKTRIČNIH VEZIJ

Matej Šalamon, Tomaž Dogša

Univerza v Mariboru, Fakulteta za elektrotehniko računalništvo in informatiko, Maribor, Slovenija

**Kjučne besede:** simulatorji električnih vezij, benchmark testiranje, neponovljivost rezultatov, kaotična vezja, Chujev oscilator, nepravilnost.

**Izvleček:** Najkvalitetnejši simulatorji SPICE, kljub svoji relativni zrelosti, zmeraj ne zagotavljajo pravilnih rezultatov, na kar opozarjajo številni znanstveni prispevki /1/, /2/, /3/, /4/, /5/, /6/, /7/.

Naš prispevek opozarja na še eno kritično nepravilnost omenjenih simulatorjev - neponovljivost rezultatov simulacij. Ugotovili smo, da se lahko ta pojavi, kadar simuliramo vezje z istim simulatorjem, inštaliranim na platformah z različnimi procesorji. Zaradi tega je smiselno preveriti, ali današnji simulatorji zagotavljajo ponovljivost rezultatov in kvantitativno ovrednotiti njihovo morebitno neponovljivost. V ta namen smo predlagali primerno testno vezje in tri stopenjsko metriko za ocenjevanje neponovljivosti, ki jo je mogoče uporabiti tudi pri ocenjevanju kakovosti simulatorjev.

# Problem of Non-repeatability of the Circuits Simulation

**Key words:** circuit simulators, benchmark testing, non-repeatability of results, chaotic circuits, Chua's oscillator, anomaly.

**Abstract:** SPICE circuit simulators are indispensable tools for integrated circuits design and for variety of scientific research activities. In spite of their mature age this simulators can give erroneous results /1/, /2/, /3/, /4/, /5/, /6/, /7/.

If we repeat the simulation on a different computer with the same simulator it is expected that results will not differ significantly. This property is called repeatability. There are a variety of situations where repeatability could be a problem. Repeated simulation can be performed with the same simulator on the same type of a computer, or with a different simulator on the same or on a different type of a computer, or with the same simulator installed on a different computer. We have focused on repeatability testing of different SPICE simulators installed on different platforms running transient analysis.

If the repeatability is not assured it is reasonable to evaluate the non-repeatability. Since deviations can occur between reference and repeated results in different ways, we have proposed three different non-repeatability measures. First order non-repeatability measure is used for the evaluation of time value deviations of time-domain waveforms. Second order non-repeatability measure evaluates dissimilarities of time-domain waveforms, and third order measure evaluates the deviation of global circuit behavior. To address this problem a functional testing of simulators were used.

Testing simulators with circuits of CircuitSim90 benchmark suite did not expose any repeatability problems. We have discovered that chaotic circuits are more efficient for the detection of non-repeatability because they are hypersensitive to the initial conditions. Chua's oscillator was selected as a representative member of chaotic circuits.

We have found out that some simulators did not ensure repeatability of results if they have been installed on different platforms. It was also discovered that the non-repeatability was most frequent if simulators were installed on the platforms with processors made by different manufactures. The consequences of non-repeatability were: significant time value deviations of time-domain waveforms and dissimilarities of their form. The type of processors however does not have significant influence on the circuit's global behavior.

The reasons for this anomaly and possibilities of its elimination were also addressed. The reason could be one or more errors in simulator's code or in the compiler, which allows different interpretations of the same processor instructions on different types of processors.

## 1. Uvod

Najkvalitetnejši simulator električnih vezij, ki se uporablja v industriji, različnih znanstveno-raziskovalnih in izobraževalnih institucijah, je simulator SPICE (Simulation Program with Integrated Circuit Emphasis). Njegovo jedro, ki je javna last, je bilo razvito med leti 1972 in 1992 na Kalifornijski Univerzi Berkeley, v sodelovanju z Bellovimi laboratoriji. Vgrajeno je v številne komercialne različice, katerih kakovost lahko primerjamo s pomočjo standardne benchmark zbirke *CircuitSim90* /8/. Najpogosteje primerjamo hitrosti simulatorjev in njihovo uspešnost pri reševanju konvergenčnih problemov /9/, /10/, /11/. Namen primerjalnih testov pa ni samo primerjanje izbranih karakteristik (npr. hitrosti, konvergence) ampak pridobiti širši vpogled v kakovost simulatorja. Primerjalni testi se lahko uporabijo tudi za merjenje uspešnosti novih in izboljšanih algoritmov /12/ ter za odkrivanje nepravilnosti simulatorjev, ki so še zmeraj prisotne.

V letu 1993 sta Angelo Brambilla in Dario D'Amore opozorila na nepravilne rezultate, ki se pojavijo z analizo prehodnega pojava pri zelo preprostih linearnih vezij. V prispevku /1/ ugotavljata, da je razlog za nepravilne rezultate hiba trapezne integracijske metode, nikakor pa ne njena implementacija ali topologija vezij ter uporabljeni modeli. Opozorila sta na frekvenčno popačenje časovnih odzivov in lažni prehodni pojav.

Velikokrat se zgodi, da rešitev ne konvergira, kar povzroči prekinitev simulacije. Ti problemi nastopijo zaradi iterativnega iskanja rešitev, predvsem pri enosmernih analizah in analizi prehodnega pojava. Charles Hymowitz v literaturi /4/ opisuje reševanje tovrstnih težav.

Avtorji prispevkov /5/ in /6/ opisujejo problematiko numeričnega integriranja na primeru vezja s pozitivno povratno vezavo. Analitično določen časovni odziv je neomejen, rezultat simulacije pa kaže, da je odziv omejen. Kot glavni vzrok nepravilnosti navajajo nepravilno izbran korak numeričnega integriranja, kar pa je mogoče odpraviti.

Posledica nepravilno izbranega koraka integriranja je lahko ne le frekvenčno popačenje /1/, ampak tudi lažno kaotično obnašanje vezij. Zaradi prevelikega dopustnega koraka numeričnega integriranja se lahko pojavi frekvenčno popačen odziv že pri preprostem linearnem LC vezju /2/, /3/. V primeru nelinearnega vezja (Colpittsovega oscilatorja) pa je odziv celo lažne kaotične narave.

Če ponovimo simulacijo, pričakujemo, da bomo dobili skoraj identične rezultate. To lastnost imenujemo ponovljivost simulacije. Ponovno simulacijo lahko izvedemo z istim simulatorjem na istem računalniku, z istim simulatorjem na drugem računalniku, ali s podobnim simulatorjem na istem ali drugem računalniku. V prispevku se bomo omejili na situacijo, ko ponovno simulacijo izvedemo z istim simulatorjem na drugem računalniku.

V tem prispevku se bomo ukvarjali s vprašanjem, ali današnji simulatorji električnih vezij zagotavljajo ponovljivost rezultatov simulacij. Problematika ponovljivosti rezultatov simulacij je opisana v drugem poglavju, v katerem je predlagana tri stopenjska metrika za kvantitativno ocenjevanje neponovljivosti rezultatov. V tretjem poglavju so opisani rezultati testiranja.

## 2. Neponovljivost simulacije

Predpostavimo, da s simulatorjem A simuliramo vezje. Rezultate te simulacije poimenujemo referenčni rezultati in jih označimo z A. Rezultate, ki jih dobimo s ponovno simulacijo istega vezja, označimo z B. Če se ti rezultati razlikujejo od referenčnih za manj kot dopuščamo, je ponovljivost zagotovljena. Kadar rezultati simulacij A in B odstopajo za več kot dopuščamo, govorimo o neponovljivosti rezultatov. Če primerjamo rezultate analize prehodnega pojava (TRAN), se odstopanja med A in B kažejo na tri načine:

1. Z različnimi vozliščnimi potenciali. Oblike časovnih potekov so identične. Bistvenih razlik v globalnem obnašanju testnega vezja ni.
2. Z različnimi vozliščnimi potenciali in različnimi oblikami časovnih potekov. Bistvenih razlik v globalnem obnašanju testnega vezja ni.
3. Z različnimi vozliščnimi potenciali, različnimi oblikami časovnih potekov in z različnim globalnim obnašanjem testnega vezja.

Z ozirom na navedene načine odstopanj, smo predlagali ti di kvantitativne ocene za: neponovljivost trenutnih vrednosti signalov - neponovljivost I. stopnje (*M1*), neponovljivost oblik signalov neponovljivost II. stopnje (*M2*) in neponovljivost globalnega obnašanja vezja - neponovljivost III. stopnje (*M3*). Naveden vrstni red ustreza stopnjevanju neponovljivosti rezultatov simulacij.

### 2.1 Mera za neponovljivost trenutnih vrednosti signalov

Rezultat analize prehodnega pojava je *m* časovnih potekov napetosti in tokov. Posamezni časovni potek je opisan z *n* trenutnimi vrednostmi. Časovne poteke napetosti in tokov, ki jih dobimo s simulacijo A, zapišimo z vrstičnimi vektorji v matriki **X**:

$$\mathbf{X}=\begin{bmatrix}\mathbf{x}_1\\ \mathbf{x}_2\\ \vdots\\ \mathbf{x}_m\end{bmatrix}=\begin{bmatrix}x_1(t_1) & x_1(t_2) & \cdots & x_1(t_n)\\ x_2(t_1) & x_2(t_2) & \cdots & x_2(t_n)\\ \vdots & \vdots & \ddots & \vdots\\ x_m(t_1) & x_m(t_2) & \cdots & x_m(t_n)\end{bmatrix}. \quad (1)$$

Z matriko **Y** na podoben način označimo rezultate simulatorja B. Namen ocene neponovljivost I. stopnje je ovrednotiti odstopanja trenutnih vrednosti časovnih potekov tokov in napetosti, ki jih dobimo pri simulaciji A in s ponovno simulacijo B. Odstopanja trenutnih vrednosti ovrednotimo s pomočjo razdalj med vrstičnimi vektorji matrik **X** in **Y**. Razdaljo med *k*-tima vrstičnima vektorjema $\mathbf{x_k}$ in $\mathbf{y_k}$ izračunamo s pomočjo enačbe:

$$d(\mathbf{x_k},\mathbf{y_k})=\sum_{i=1}^{n}\left|x_k(t_i)-y_k(t_i)\right|. \quad (2)$$

Komponente vektorja $\mathbf{x_k}$ naj bodo referenčne, komponente vektorja $\mathbf{y_k}$ pa tiste, ki jih z referenčnimi primerjamo. Vsaka komponenta vektorja $\mathbf{y_k}$ se sme razlikovati od komponente vektorja $\mathbf{x_k}$ za največ $\Delta x$. Če je $\Delta x$ *dopustno odstopanje* komponent vektorja $\mathbf{y_k}$ od komponent vektorja $\mathbf{x_k}$ izraženo v odstotkih, je *dopustna razdalja* med *k*-tima vektorjema $\mathbf{x_k}$ in $\mathbf{y_k}$ določena z enačbo:

$$\varepsilon_k=\begin{cases}\dfrac{|\Delta x|}{100}\displaystyle\sum_{i=1}^{n}|\zeta| & ;x_k(t_i)=0 \quad i=1,2\ldots n\\ \dfrac{|\Delta x|}{100}\displaystyle\sum_{i=1}^{n}|x_k(t_i)| & ;sicer\end{cases}, \quad (3)$$

pri čemer je $\zeta$ minimalna, od nič različna, v računalniku predstavljiva, vrednost.

Privzemimo, da je dopustno odstopanje $\Delta x$ za vse pare primerjanih vrstičnih vektorjev matrik **X** in **Y** enako. Rezultati simulacij A in B so *ponovljivi* le, če so razdalje med vsemi primerjanimi časovnimi poteki manjše ali enake dopustnim:

$$\varepsilon_1\geq d(\mathbf{x_1},\mathbf{y_1})\wedge\varepsilon_2\geq d(\mathbf{x_2},\mathbf{y_2})\wedge\ldots\wedge\varepsilon_m\geq d(\mathbf{x_m},\mathbf{y_m}). \quad (4)$$

Kadar ta pogoj ni izpolnjen, so rezultati simulacij *neponovljivi*. Za kvantitativno oceno neponovljivosti I. stopnje predlagamo naslednjo mero:

$$M1 = \sqrt{\sum_{k=1}^{m} d(\mathbf{x}_k, \mathbf{y}_k)^2} \quad (5)$$

Vrednost *M1* je tem večja, čim več je odstopanj med trenutnimi vrednostmi časovnih potekov in čim večja so. Če želimo primerjati neponovljivost, ki se pojavi pri različnih testnih vezij, moramo *M1* ustrezno normirati. Normiranje lahko izvedemo tako, da posamezno oceno *M1* normiramo z normo vektorja dopustnih razdalj:

$$M1^* = \sqrt{\sum_{k=1}^{m} \varepsilon_k^{\,2}} = \frac{|\Delta x|}{100} \sqrt{\sum_{k=1}^{m} \left( \sum_{i=1}^{n} |x_k(t_i)| \right)^2} . \quad (6)$$

Če izberemo zadostno majhen $\Delta x$ in ne pride do neponovljivosti, potem bo tudi zagotovljena ponovljivost oblik in globalnega obnašanja.

## 2.2 Mera za neponovljivost oblik signalov

*M2* se nanaša na obliko časovnih potekov napetosti oziroma tokov. Ker so lahko rezultati simulacij A in B oblikovno podobni tudi, če so vzorci trenutnih vrednosti primerjanih časovnih potekov med seboj nekoliko zamaknjeni, smo za ocenjevanje oblikovnega odstopanja uporabili maksimalno vrednost križnokorelacijskih funkcij $r_{xkyk(j)}$ vseh *m* časovnih potekov.

Časovna poteka $\mathbf{x_k}$ in $\mathbf{y_k}$ sta maksimalno korelirana, ko križnokorelacijska funkcija $r_{xkyk(j)}$ zavzame maksimalno ekstremno vrednost. Če je ta +1 obstaja med $\mathbf{x_k}$ in $\mathbf{y_k}$ popolna pozitivna koreliranost, če je ta vrednost -1, obstaja med njima popolna inverzna koreliranost, če pa je 0, med $\mathbf{x_k}$ in $\mathbf{y_k}$ ni linearne povezave.

Časovna poteka $\mathbf{x_k}$ in $\mathbf{y_k}$ sta oblikovno tem manj podobna, čimbolj je maksimalna vrednost križnokorelacijske funkcije $r_{xkyk(j)}$ oddaljena od vrednosti +1. Če je maksimalna vrednost križnokorelacijske funkcije $r_{xkyk(j)} \leq 0$, sta časovna poteka $\mathbf{x_k}$ in $\mathbf{y_k}$ oblikovno nepodobna.

Oblikovno nepodobnost primerjanih časovnih potekov lahko ocenimo s pomočjo naslednje mere:

$$M2 = 1 - \frac{1}{m} \sum_{k=1}^{m} r_k , \quad (7)$$

pri čemer je $r_k$ maksimalna vrednost križnokorelacijske funkcije:

$$r_k = \begin{cases} \max\limits_j \left( r_{xkyk}(j) \right) & ; \max\limits_j \left( r_{xkyk}(j) \right) > 0 \\ 0 & ; \max\limits_j \left( r_{xkyk}(j) \right) \leq 0 \end{cases}$$

$$\text{za } j = -(n-1), -(n-2), \ldots, 0, 1, 2, \ldots (n-1). \quad (8)$$

Neponovljivost oblik signalov je tem večja, čim večja je vrednost *M2*, ki je lahko iz intervala [0,+1].

Primerjana časovna poteka $\mathbf{x_k}$ in $\mathbf{y_k}$ sta podobna, če je vrednost $r_k$ večja ali enaka *minimalni dopustni vrednosti* $r_{min}$, ki lahko zavzame vrednosti iz intervala (0,+1]. Če to velja za vse primerjane časovne poteke:

$$r_{\min} \leq r_1 \wedge r_{\min} \leq r_2 \wedge \ldots \wedge r_{\min} \leq r_m , \quad (9)$$

se oblike napetosti oziroma tokov, dobljenih s ponovno simulacijo, bistveno ne razlikujejo od referenčnih.

## 2.3 Mera za neponovljivost globalnega obnašanja

Namen ocenjevanja neponovljivosti III. stopnje je ovrednotiti odstopanja med globalnim obnašanjem testnega vezja pri referenčni simulaciji A in ponovni simulaciji B. Globalno obnašanje testnega vezja ocenimo na osnovi njegovih značilnih lastnosti - bistvenih lastnosti, s katerimi je mogoče okarakterizirati in oceniti njegovo obnašanje. Tipične značilne lastnosti so: pasovna širina, vhodna upornost, preklopna napetost, harmonska popačenja, frekvenca osciliranja itd.

Odstopanja med globalnim obnašanjem testnega vezja pri simulaciji A in ponovni simulaciji B bodo tem večja, čim večja bodo odstopanja med njegovimi istovrstnimi značilnimi lastnostmi. Ker imajo lahko različna vezja različne in različno število značilnih lastnosti, je mera za neponovljivosti III. stopnje odvisna od vrste vezja.

Ker smo pri testiranju ponovljivosti uporabili kaotična testna vezja, smo to mero natančno definirali za tovrstna vezja. Za značilno lastnost smo izbrali mejo med kaotičnim in ne kaotičnim režimom delovanja.

S pomočjo simulatorja A določimo *m* bifurkacijskih točk: $a_1, a_2, \ldots a_m$, ki nastopijo pri bifurkacijah s podvojitvijo periode in jih odčitamo iz bifurkacijskega diagrama (slika 1). Ta predstavlja odvisnost maksimalnih vrednosti izbrane spremenljivke stanja v vezju od bifurkacijskega parametra tj. parametra, s katerim lahko vplivamo na kvalitativne spremembe v obnašanju vezja.

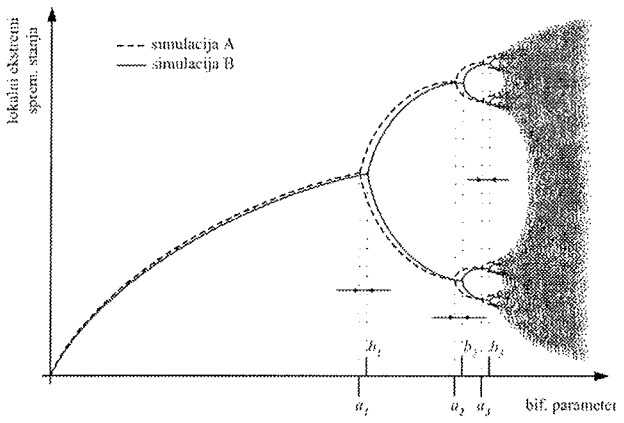


*Slika 1: Bifurkacijska diagrama, ki ju dobimo s pomočjo rezultatov simulacij A in B.*

Mejo med kaotičnim in ne kaotičnim režimom /13/ določa enačba:

$$a_\infty = (a_2 - a_1)\cdot\left(\frac{1}{\delta_a - 1}\right) + a_2. \qquad (10)$$

Pri tem je $\delta_a$ Feigenbaumova konstanta, ki jo izračunamo s pomočjo izraza:

$$\delta_a = \lim_{k\to m} \frac{a_k - a_{k-1}}{a_{k+1} - a_k} \approx \frac{a_m - a_{m-1}}{a_{m+1} - a_m}. \qquad (11)$$

Na podoben način določimo mejo kaotičnosti $b_\infty$, ki jo izračunamo iz podatkov, dobljenih s ponovno simulacijo.

Za oceno nepodobnosti med globalnim obnašanjem testnega vezja predlagamo naslednjo mero[1]:

$$M3 = \left|\frac{a_\infty - b_\infty}{a_\infty}\right| \cdot 100\ [\%]. \qquad (12)$$

Nepodobnost globalnega obnašanja testnega vezja je tem večja, čim večja so odstopanja med mejnima vrednostma $a\infty$ in $b\infty$.

Predpostavimo, da je globalno obnašanje testnega vezja, določeno s simulacijo B še podobno globalnemu obnašanju določenim s simulacijo A, če meja med kaotičnim in ne kaotičnim režimom delovanja vezja v obeh primerih ne odstopa za več kot Δ[%]:

$$a_\infty - \frac{a_\infty \cdot \Delta}{100} \le b_\infty \le a_\infty + \frac{a_\infty \cdot \Delta}{100}. \qquad (13)$$

Če pogoj (13) ni izpolnjen, je globalno obnašanje testnega vezja popolnoma nepodobno kar pomeni, da so rezultati simulacij *totalno neponovljivi*.

## 3. Testiranje ponovljivosti rezultatov simulacij

Testirali smo ponovljivost rezultatov simulatorja, ki je bil inštaliranih na platformah z različnimi procesorji. Ker je bila uporabljena ista izvršna koda, smo pričakovali, da bodo rezultati ponovnih simulacij popolnoma enaki referenčnim. Ugotovili smo, da vezja iz standardne benchmark zbirke *CircuitSim90* niso zaznala nobene neponovljivosti. Ker so kaotična vezja hiperobčutljiva na začetne pogoje, smo za testiranje ponovljivosti izbrali Chujev oscilator (slika 2).

Ugotovili smo, da je detekcija neponovljivosti uspešna le:
1. če je obnašanje testnega vezja kaotično in,
2. če je izbran dovolj velik čas trajanja analize prehodnega pojava.

Dejanska neponovljivost lahko ostane nezaznavna:
1. če je osciliranje Chujevega oscilatorja periodično, ali
2. če je kljub kaotičnemu režimu delovanja, izbran prekratek čas trajanja analize prehodnega pojava (glej sliko 3).

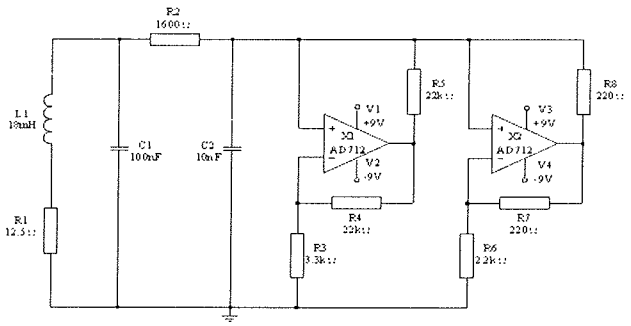


*Slika 2: Chujev oscilator /14/ - testno vezje za testiranje ponovljivosti rezultatov simulacij.*

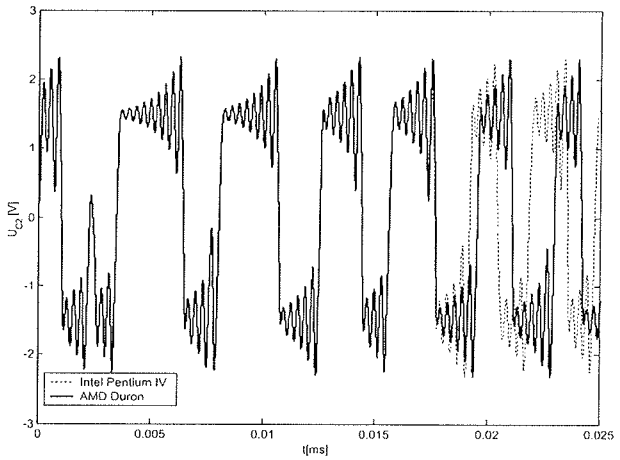


*Slika 3: Divergenca časovnih potekov napetosti na kondenzatorju C2 v Chujevem oscilatorju, (R2=1600Ω), simuliranem na platformi s procesorjem AMD Duron in Intel Pentium IV, je zelo očitna šele po približno 17.5ms.*

Podobne rezultate smo dobili tudi z drugimi kaotičnimi vezji. Testiranje smo izvedli na raznih platformah in z različnimi verzijami simulatorja SPICE proizvajalcev: *Intusoft, OrCAD, PENZAR Development, Linear Technology Corporation, FERI Ljubljana* - skupina *CAD* in *Mentor Graphics*. Le pri nekaj simulatorjih se problem neponovljivosti ni pojavil.

### 3.1 Ocene neponovljivosti trenutnih vrednosti signalov

V poglavju 2.1 smo privzeli, da bodo rezultati simulacij ponovljivi, če nobena od razdalj med referenčnimi časovnimi poteki in časovnimi poteki, ki jih dobimo pri ponovnih simulacijah, ne presega dopustne. Pri testiranju smo privzeli, da je dopustno odstopanje trenutnih vrednosti primerjanih časovnih potekov Δx enako ±0.01%.

Ocene neponovljivosti rezultatov simulacij, ki smo jih dobili pri testiranju enega izmed simulatorjev SPICE, inštaliranega na platformah z različnimi procesorji, so zapisane v tabeli 1 in so podane v normirani obliki *M1/M1**.

1 *Ker v primeru predlaganega testnega vezja mejna vrednost bifurkacijskega parametra $a_\infty$ ne more biti nič, smo M3 definirali kot relativna odstopanja med vrednostma $a_\infty$ in $b_\infty$.*

*Tabela 1: Ocene M1/M1* za enega izmed simulatorjev SPICE, inštaliranega na platformah z različnimi procesorji.*

| **Referenčna platforma A s procesorjem** | **Platforma B s procesorjem** | | | | | | |
|---|---|---|---|---|---|---|---|
| | *Cyrix (IBM) 6x86MX* | *AMD Duron* | *AMD Athlon XP* | *Intel Pentium MMX* | *Intel Pentium III* | *Intel Celeron (Willamette)* | *Intel Pentium IV* |
| *Cyrix (IBM) 6x86MX* | - | 12099.93 | 12099.93 | 11905.79 | 11905.79 | 11905.79 | 11905.79 |
| *AMD Duron* | 12082.59 | - | 0 | 11782.12 | 11782.12 | 11782.12 | 11782.12 |
| *AMD Athlon XP* | 12082.59 | 0 | - | 11782.12 | 11782.12 | 11782.12 | 11782.12 |
| *Intel Pentium MMX* | 11991.36 | 11883.84 | 11883.84 | - | 0 | 0 | 0 |
| *Intel Pentium III* | 11991.36 | 11883.84 | 11883.84 | 0 | - | 0 | 0 |
| *Intel Celeron (Willamette)* | 11991.36 | 11883.84 | 11883.84 | 0 | 0 | - | 0 |
| *Intel Pentium IV* | 11991.36 | 11883.84 | 11883.84 | 0 | 0 | 0 | - |

Ocene v tabeli 1 kažejo, da daje simulator:

1. neponovljive rezultate, če je inštaliran na platformah s procesorji različnih proizvajalcev;
2. ponovljive rezultate, če je inštaliran na platformah s procesorji istega proizvajalca - vrednosti *M1/M1** so enake nič.

## 3.2 Ocene neponovljivosti oblik signalov

Z ocenjevanjem neponovljivosti II. stopnje smo ocenili oblikovno nepodobnost primerjanih časovnih potekov. Ker postane morebitna divergenca primerjanih časovnih potekov očitna šele po približno 50ms smo privzeli, da sta dva časovna poteka od tedaj oblikovno podobna, če je maksimalna vrednost pripadajoče križnokorelacijske funkcije večja ali enaka 0.8. Če je pri tem pogoj (9) zmeraj izpolnjen, simulator zagotavlja oblikovno podobne časovne poteke.

V tabeli 2 so podane ocene neponovljivosti II. stopnje za enega izmed simulatorjev.

Glede na dobljene rezultate lahko zaključimo, da simulator zagotavlja oblikovno podobne časovne poteke napetosti in tokov v testnem vezju le, če je inštaliran na platformah z procesorjem istega proizvajalca. Vrednosti v tabeli 2 namreč kažejo, da je v teh primerih vrednost *M2* enaka nič, v ostalih primerih pa pogoj (9) ni izpolnjen.

## 3.3 Ocene neponovljivosti globalnega obnašanja

Ocena neponovljivosti III. stopnje vrednoti odstopanja v globalnem obnašanju testnega vezja. Po definiciji, opisani v poglavju 2.3, odstopanja ocenimo z odstopanjem meje med kaotičnim in ne kaotičnim režimom delovanja.

Pri ocenjevanju neponovljivosti III. stopnje smo se omejili na prve tri bifurkacijske točke. Za bifurkacijski parameter smo izbrali upornost R2, za opazovano spremenljivko stanja pa napetost kondenzatorju C2. Upornost R2 smo spreminjali na intervalu $1820\Omega \leq R2 \leq 1860\Omega$ po koraku $0.2\Omega$ in v dobljenih časovnih potekih napetosti na kondenzatorju C2,

*Tabela 2: Ocene neponovljivosti II. stopnje za enega izmed simulatorjev, inštaliranega na platformah z različnimi procesorji.*

| **Referenčna platforma A s procesorjem** | **Platforma B s procesorjem** | | | | | | |
|---|---|---|---|---|---|---|---|
| | *Cyrix (IBM) 6x86MX* | *AMD Duron* | *AMD Athlon XP* | *Intel Pentium MMX* | *Intel Pentium III* | *Intel Celeron (Willamette)* | *Intel Pentium IV* |
| *Cyrix (IBM) 6x86MX* | - | 0.8437 | 0.8437 | 0.8354 | 0.8354 | 0.8354 | 0.8354 |
| *AMD Duron* | 0.8437 | - | 0 | 0.8117 | 0.8117 | 0.8117 | 0.8117 |
| *AMD Athlon XP* | 0.8437 | 0 | - | 0.8117 | 0.8117 | 0.8117 | 0.8117 |
| *Intel Pentium MMX* | 0.8354 | 0.8117 | 0.8117 | - | 0 | 0 | 0 |
| *Intel Pentium III* | 0.8354 | 0.8117 | 0.8117 | 0 | - | 0 | 0 |
| *Intel Celeron (Willamette)* | 0.8354 | 0.8117 | 0.8117 | 0 | 0 | - | 0 |
| *Intel Pentium IV* | 0.8354 | 0.8117 | 0.8117 | 0 | 0 | 0 | - |

*Tabela 3: Ocene neponovljivosti III. stopnje za enega izmed simulatorjev SPICE, inštaliranega na platformah z različnimi procesorji.*

| **Referenčna platforma A s procesorjem** | **Platforma B s procesorjem** | | | | | | |
|---|---|---|---|---|---|---|---|
| | *Cyrix (IBM) 6x86MX* | *AMD Duron* | *AMD Athlon XP* | *Intel Pentium MMX* | *Intel Pentium III* | *Intel Celeron (Willamette)* | *Intel Pentium IV* |
| *Cyrix (IBM) 6x86MX* | - | $9.665\ 10^{-4}$ | $9.665\ 10^{-4}$ | $9.665\ 10^{-4}$ | $9.665\ 10^{-4}$ | $9.665\ 10^{-4}$ | $9.665\ 10^{-4}$ |
| *AMD Duron* | $9.665\ 10^{-4}$ | - | 0 | 0 | 0 | 0 | 0 |
| *AMD Athlon XP* | $9.665\ 10^{-4}$ | 0 | - | 0 | 0 | 0 | 0 |
| *Intel Pentium MMX* | $9.665\ 10^{-4}$ | 0 | 0 | - | 0 | 0 | 0 |
| *Intel Pentium III* | $9.665\ 10^{-4}$ | 0 | 0 | 0 | - | 0 | 0 |
| *Intel Celeron (Willamette)* | $9.665\ 10^{-4}$ | 0 | 0 | 0 | 0 | - | 0 |
| *Intel Pentium IV* | | | | | | | |

poiskali lokalne maksimume. Njihovo odvisnost od vrednosti upornosti R2 smo opisali z bifurkacijskim diagramom.

S pomočjo enačbe (12) smo ocenili neponovljivosti III. stopnje, ki so zapisane v tabeli 3. Z ozirom na pogoj, opisan z enačbo (13), smo predpostavili, da so rezultati, ki jih daje simulator na referenčni platformi A in platformi B totalno neponovljivi, če je odstopanje med mejno vrednostjo bifurkacijskega parametra $a_\infty$ in $b_\infty$ večje od $\Delta=\pm 10\%$.

Na osnovi rezultatov ocenjevanja neponovljivosti III. stopnje smo ugotovili, da simulator, inštaliran na platformah z obravnavanimi procesorji, ne daje totalno neponovljivih rezultatov, saj je pogoj (13) v vseh primerih izpolnjen.

## 4. Sklep

V prispevku smo se ukvarjali s vprašanjem: ali današnji simulatorji električnih vezij zagotavljajo ponovljivost rezultatov simulacij? Ponovljivost rezultatov simulacij je zagotovljena takrat, kadar dobimo pri ponovitvi simulacije rezultate, ki so znotraj dopustnih odstopanj. Odstopanja med referenčnimi rezultati in rezultati ponovne simulacije se kažejo v različnih trenutnih vrednosti, v različnih oblikah potekov napetosti oziroma tokov in v različnem globalnem obnašanju vezja. Za te tri primere smo definirali ustrezne metrike, s katerimi lahko tudi ocenjujemo morebitno stopnjo neponovljivosti.

V prispevku smo se omejili na situacijo, ko ponovno simulacijo izvedemo z istim simulatorjem na drugem računalniku. Računalnika sta se razlikovala samo v vrsti mikroprocesorja, uporabljala pa sta isto izvršno kodo simulatorja. Kljub tej razliki, ki naj ne bi vplivala na rezultate simulacije, smo ugotovili, da v nekaterih primerih prihaja do neponovljivosti rezultatov simulacij. Ugotovili smo, da z vezji iz benchmark zbirke *CircuitSim90* ni možno zaznati neponovljivosti. Le pri simulaciji kaotičnih vezij se je pojavila neponovljivost trenutnih vrednosti in oblik signalov.

Na osnovi rezultatov testiranja ponovljivosti lahko zaključimo, da nekateri današnji simulatorji električnih vezij, na platformah z določenimi procesorji, ne zagotavljajo ponovljivih rezultatov in, da je neponovljivost mogoče zaznati le s pomočjo hiperobčutljivih testnih vezij. Ker benchmark zbirka *CircuitSim90* tovrstnih vezij ne vsebuje, predlagamo njeno razširitev s kaotičnim vezjem.

Vzrok za neponovljivost rezultatov je lahko ena ali več napak v programu simulatorja ali prevajalniku programa, ki dopuščajo različno interpretacijo istih procesorskih ukazov na različnih procesorjih. To je mogoče, saj se proizvajalci današnjih procesorjev do potankosti ne držijo IEEE standardov za aritmetiko s plavajočo vejico. Zraven tega nekatere lastnosti te aritmetike niso natančno specificirane, kar dopušča različnost implementacij. Proizvajalci procesorjev v svoje izdelke vgrajujejo tudi lastne dodatke, ki jih trenutni standardi ne obravnavajo.

Obstoj neponovljivosti rezultatov simulatorjev SPICE predstavlja njihovo novo nepravilnost, ki pa v mnogih primerih ostaja uporabniku prikrita.

## 5. Literatura

/1/ A. Brambilla, D. D'Amore: *The simulation Errors Introduced by Spice Transient Analysis*, IEEE Transaction Circuits and Systems-I: Fundamental theory and applications, letnik 40, št. 1, januar 1993, str. 57-60.

/2/ B. Peršič, I. Medič: *Chaotic Results of SPICE Simulator*, Proceedings of ECCTD '97, str. 1226-1230, Budapest 1997.

/3/ B. Peršič N. Basarič: *Frequency warping and chaotic behaviour generated by Spice*, Informacije MIDEM, letnik 31, št. 1, marec 2001, str. 26-32.

/4/ C. Hymowitz: *Step-by-step procedures help you solve Spice convergence problems*, EDN Magazine, marec 1994.

/5/ P. Kinget, J. Crols, M. Ingles, E. Peluso: *Are Circuit Simulators Becoming Too Stable*, IEEE Circuits and Devices Magazine, letnik 10, št. 3, str. 50, maj 1994.

/6/ B. Peršič: *Primer napačnega delovanja numerične integracije simulatorja SPICE*, Elektrotehniški vestnik, letnik 62, št. 2, leto 1995, str. 117-125.